Collisionless Coupling of Ion and Electron Temperatures in Counterstreaming Plasma Flows

J. S. Ross, H.-S. Park, R. Berger, L. Divol, N. L. Kugland, W. Rozmus, D. Ryutov, and S. H. Glenzer

Collisionless Coupling of Ion and Electron Temperatures in Counter-streaming Plasma Flows

J. S. Ross[1], H.-S. Park[1], R. Berger[1], L. Divol[1], N. L. Kugland[1], W. Rozmus[1,2], D. Ryutov[1], and S. H. Glenzer[1]

[1]*Lawrence Livermore National Laboratory, P.O. Box 808, Livermore, California 94551 and*
[2]*Department of Physics, University of Alberta Edmonton, Alberta, Canada T6G 2R3*

Rapid electron and ion heating is observed in collisionless counter-streaming plasma flows and explained via a novel heating mechanism that couples the electron and ion temperatures. Recent experiments measure plasma conditions 4 mm from the surface of single foil (single plasma stream) and double foils (two counter-streaming plasmas) targets using Thomson scattering. Significant increases in electron and ion temperatures (from < 100 eV to > 1 keV) compared to the single foil geometry are observed. While electrons are heated by friction on opposite going ions, ion-ion collisions can not explain the observed ion heating. Also, density and flow velocity measurements show negligible slow down and rule out stagnation. The nonlinear saturation of an acoustic 2-stream electrostatic instability is predicted to couple the ion temperature to the electron temperature through the dynamic evolution of the instability threshold. Particle-in-cell simulations including both collisional and collisionless effects are compared to the experimental measurements and show rapid electron and ion heating consistent with the experimental measurements.

High velocity counter-streaming plasma flows are an active area of research focused on studying collisional [1, 2] and collisionless [3–5] effects in laser produced plasmas. The interaction region is a new area for laboratory astrophysics research to investigate collisionless shocks relevant to astrophysical observations [6–8]. Particle acceleration at the front of a collisionless shock generated after a supernova explosion is a possible source of cosmic rays [9, 10]. Laboratory astrophysics experiments present a unique opportunity to study shock generation mechanisms and directly measure high-energy particle generation. Modeling of these systems is another important aspect of the project and particle-in-cell simulations are typically used for collisionless systems [11, 12]. In the case of collision dominated interactions a fluid treatment is more common [13]. These systems present an ideal platform for studying plasma evolution in the presence of electro-static and electro-magnetic instabilities.

In this Letter, we present direct measurements of rapid ion and electron heating in counter-streaming interpenetrating plasma flows. We have measured the ion and electron temperatures as well as the plasma flow velocity and electron density using Thomson scattering [14–16]. We observe less than a 10% decrease in flow velocity relative to the single foil free streaming case during the rapid heating phase. We elucidate a new ion and electron temperature coupling mechanism via direct experimental measurements of free-streaming counter-propagating plasma flows. These measurements are consistent with 2D particle-in-cell simulations including both collisional and collisionless effects.

Two plasmas are observed to stream through each other with only a small decrease of velocity and a 2-fold increase in density consistent with a mere overlap of the plasmas. Unlike previous experiments [1, 16, 17] it is clear from the flow velocity and electron density mea-
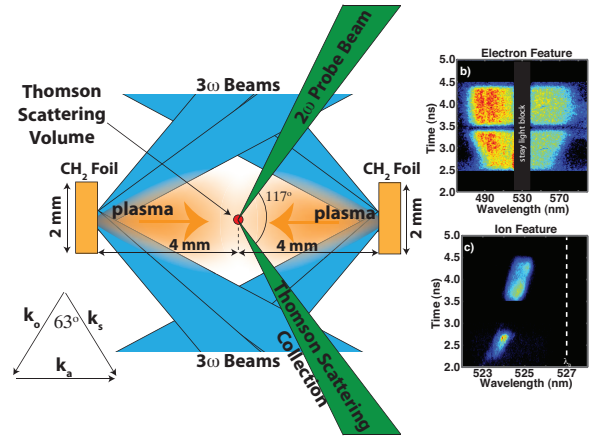

FIG. 1. (Color Online) The experimental setup is shown for the double foil configuration. Each foil is irradiated with ten 351 nm (3ω), laser beams using 1 ns square pulses with 250 μm focal spots. A 527 nm (2ω) probe beam is focused at the target chamber center. Thomson scattered light is collected 117° relative to the probe. This Thomson scattering geometry results in a matched k-vector normal to the target surface.

surements that stagnation, a rapid decrease in the flow velocity and an increase in the local density, is not a factor for these conditions. In this study, we attribute the measured increase in electron and ion temperatures to a novel combination of collisional electron heating via electron-ion drag and collisionless ion heating via an ion 2-stream instability.

The experiments have been performed at the Omega Laser at the Laboratory for Laser Energetics. Two target configurations have been used. A single foil configuration and a double foil configuration using a pair of CH$_2$ foils (2 mm in diameter and 0.5 mm thick, Fig. 1) irradiated with ten 351 nm laser beams each using 1 ns square pulses.
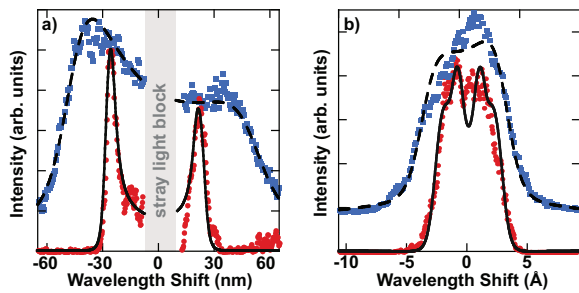
FIG. 2. (Color Online) The Thomson scattering cross section (black lines for single foil target, dashed black lines for double foil target) is fit to the measured Thomson scattering (a) electron feature and (b) ion feature at 3.5 ±0.1 ns from both the single (red circles) and double foil (blue squares) targets. The double foil data and fit are offset in intensity for clarity. The ion features are normalized to the center of the scattered signal to facilitate comparison.

Phase plates produce focal spots of 250 μm diameter. The foils are separated by 8 mm. Thomson scattering at the center point between the foils characterize the plasma conditions. The 1 ns square 527 nm probe beam timing is varied from 2 ns to 8.8 ns after the heaters beams to measure the plasma conditions at different times over 1 ns long intervals that are determined by the duration of the Thomson scattering probe.

The Thomson scattered light has been collected at an angle of 116.8° from the incident probe beam direction. The scattered light was imaged onto the entrance slit of a pair of spectrometers. A 1 m spectrometer with a magnification of 1.5:1, a 2400 lines/mm grating and a 200 μm entrance slit provides a spectral resolution of 0.056 nm for measuring the ion feature. A 1/3-meter spectrometer with a magnification of 0.9:1, a 150 lines/mm grating, and a 100 μm entrance slit was used to measure the electron feature with a spectral resolution of 3.6 nm. A Hamamatsu 7700 streak camera was coupled to the output of both spectrometers resulting in a temporal resolution of 200 ps for the 1 m system and 100 ps for the 1/3 m system, in both cases limited by the temporal dispersion of the spectrometer. The Thomson scattering volume was defined by the overlap of both slit images, the streak camera slit and the spectrometer slit, in the plasma (150μm×150μm for the 1-meter system and 110μm×110μm for the 1/3-meter system) with the probe beam (70μm diameter).

The raw Thomson scattered spectra is shown in Figure 1 (b) and (c). The electron feature [Fig. 1 (b)] measures the electron temperature and density when fitted with the Thomson scattering form factor [15]. Figure 2 shows a comparison of scattered spectra from the single foil and double foil targets. The electron temperature (T_e) and the electron density (N_e) are measured with an uncertainty of ±15% from the electron feature [Fig. 2 (a)]. The carbon ion temperature (T_i) and plasma flow veloc-

ity (U) are then measured from the ion feature [Fig. 2 (b)]. The plasma flow velocity has been measured with an accuracy of ±10%, in the double foil configuration the Thomson scattering form factor is calculated with a sum of Maxwellian distributions separated in velocity space by plus and minus the plasma flow velocity. The carbon ion temperature uncertainty has been determined independently for each time based on the quality of the fit, an example fit is shown in Fig. 2 (b). The Thomson scattered signal is only sensitive to the carbon ion temperature in this regime, it is insensitive to the hydrogen ion temperature.

The measured plasma conditions are shown in Figure 3 for a single foil configuration and a double foil configuration. As the two plasmas interpenetrate, distinct Doppler-shifted scattering signals are observed, corresponding to two streams. A decrease of ∼10% in the flow velocity is observed between the double and single foil configurations, a clear indication that stagnation or fully formed shocks are not present during the experiment. This is also evident in the electron density measurement [Fig. 3 (b)] were the double foil configuration shows an increase in density of no more than a factor of two compared to the single foil configuration.

Figure 3 (c) and (d) show the measured ion and electron temperatures respectively compared with simulations. A rapid and significant increase in both temperatures in the double foil configuration is observed compared to the single foil configuration. Purely collisional heating is assessed for these conditions[14] and does not reproduce the observed increase in ion temperature [Fig. 3 (c)].

A detailed modeling of these experiments requires the inclusion of both collisional (fluid) and collisionless (kinetic) effects. Taking typical parameters $N_e = 4 \times 10^{18}$ cm^{-3}; $T_e = 300$eV; $T_i = 100$eV; $U/c = 0.005$ and assuming fully ionized carbon ions, we have $v_e/c = 0.024 \gg U/c = 0.005 \gg v_i/c = 10^{-4}$ (i.e. electrons are mostly adiabatic while the kinetic energy of the flow is much greater than the ion internal energy) where v_e and v_i are the electron and ion thermal velocities respectively. Collisional effects are evident in the relative rates of transfer of flow energy into electron thermal energy due to Joule heating $(U/v_e)^2\nu_e \approx 0.01ps^{-1} \gg (U/v_i)^2\nu_{i+/i-} \approx 0.001$ps^{-1}, where $\nu_{i+/i-}$ is the collision frequency between ions from counterstreaming flows. As far as collisional coupling is concerned, one can expect the counterstreaming plasmas to freely interpenetrate ($U \gg v_i$), while T_e will rise over a few 100 ps due to friction and T_i will remain cold [14].

Plasma instabilities (collisionless effects) dramatically alter this collision-only result. One can estimate the plasma instability growth rates as $\gamma_{ac} \approx \omega_{pi} = 2$ and $\gamma_w \approx \omega_{pi}U/c = 0.01$ (all rates are in units of 10^{12} s^{-1}) where γ_{ac} is the growth rate for the electrostatic two-stream instability [18] and γ_w for the electromagnetic
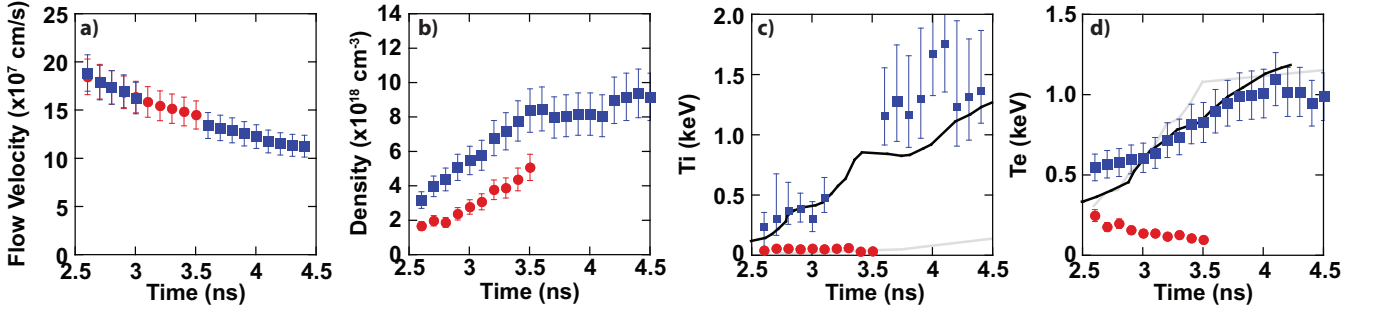
FIG. 3. (Color Online) The plasma flow velocity (a), electron density (b), carbon ion temperature (c), and electron temperature (d) are measured using Thomson scattering for the single foil (red circles) and double foil (blue squares) configurations. The electron and ion temperatures are compared to a simple analytic model [14] assuming equal carbon and hydrogen ion temperatures (grey line). Temperatures from 2D collisional PIC simulations (black line) are also shown.

Weibel instability [3]. The 2-stream instability will heat the ions over a few ps until $T_{i\perp} \approx T_e$ ($T_{i\perp}$ denotes the ion temperature perpendicular to the plasma flow direction and $T_{i\|}$ denotes the temperature parallel to the flow), the ions will then relax to a Maxwellian distribution over tens of ps due to the ion-ion Coulomb collisions within each flow. This increase in T_i will further limit the (already slow) growth of the Weibel instability which should not play an energetically important role over less than a nanosecond. As T_e keeps increasing due to friction, the 2-stream instability will develop again and keep T_i close to the threshold value ($T_i \sim 1.18T_e$). In this system, a plasma instability provides a new way of coupling the ion temperature with the electron temperature as the later evolves due to collisional effects. A modeling that accounts for only collisional effects and ignores collective processes will miss this coupling and underestimate T_i, while a collisionless kinetic treatment will miss the increase in T_e.

A theoretical calculation of the acoustic-two-stream instability growth rate (γ_{ac}) and the saturation of the 2-stream acoustic instability by ion heating is a key to explaining the evolution of T_i in this experiment where no stagnation occurs. The acoustic-two-stream instability growth rate for 2 multi-species counter-streaming plasmas is the (real) root γ_{ac} of,

$$\epsilon = 1 + \alpha^2 - \sum_i \frac{\alpha^2 f_i Z_i^2 T_e}{2\bar{Z}T_i} Re\left[Z'\left(\frac{i\gamma_{ac}+\sin\theta U}{\sqrt{2}v_i}\right)\right] = 0,$$
(1)

where $\alpha = 1/k\lambda_D$, λ_D is the debye length, f_i is the fraction of ions of species i, and $\bar{Z} = \sum Z_i f_i$. As $Re[Z']$ is bounded on the imaginary axis, with $\text{Max}_{\gamma>0} Re[Z'(i\gamma)] \approx 0.57$, there is a maximum value of T_i (all other parameters fixed) for which an unstable root exists. For a CH_2 plasma, one can neglect the contribution of hydrogen in Eq. (1) and the collisionless threshold is mostly set by the carbon ion temperature ($Z_i=6, A_i=12, f_i=1/3$) due to the Z_i^2 dependence. Near threshold, Eq. (1) can be written as

$\epsilon \approx 1 + \alpha^2 - 0.57\alpha^2\frac{9T_e}{4T_i}$. As T_i increases, the unstable modes are at longer and longer wavelength ($\alpha \to \infty$) until a threshold at $T_i \approx 1.18T_e$ is reached and all acoustic modes are stable. The maximum of the plasma dispersion function (Z') on the real axis is reached for $\sin\theta \approx 2.1v_i/U$, which is almost perpendicular to the flow. Trapping of C ions and diffusion in a broad spectrum of acoustic waves will lead to an increase of the carbon ion temperature (T_c) in the transverse direction [18]. While all collision rates are small compared to the initial (cold) growth rate γ_{ac}, the C-C equilibration rate is important for saturation near threshold.

The maximum growth rate near threshold is obtained by maximizing γ_{ac} over the acoustic wave vector k as T_i increases towards the threshold. One finds $\frac{\gamma_{th}}{\omega_{pi}} = \frac{2}{3}\Delta^{3/2}$, with $\Delta = 0.57 - \frac{4T_i}{9T_e}$. This can be compared to the thermal equilibration rate for carbon ions [19] to find the collisional threshold,

$$\frac{\gamma_{th}}{\omega_{pi}} = \frac{2}{3}\Delta^{3/2} \geq \frac{\nu_{cc}}{\omega_{pi}} \approx \frac{6.3 10^{-12}N_c[cm^{-3}]^{1/2}\ln\Lambda Z_c^3}{T_{c_\|}^{3/2}[eV]}.$$

For the above parameters, ion-ion collisions will reduce the peak ion temperature by 20 percent compared to the collisionless estimate ($T_i \sim T_e$). At higher densities or for higher Z ions, weak collisions can significantly lower the final ion temperature and should not be neglected in simulations. To confirm our theoretical scenario, we use a particle-in-cell code (PSC [20]) that includes binary inter and intra species collisions using the method of [21]. We setup the simulations with 2 counter-streaming plasmas of $C(A_i = 12, Z_i = 6) and H_2(A_i = 1, Z_i = 1)$ starting with $N_e = 2 \times 10^{18}$ cm^{-3}; $T_e = 300$ eV; $T_i = 100$ eV; $U/c = 0.005$. The simulations box is 24 μm by 36 μm with 24 cells per micron and 1000 particles per cell. We used third-order splines and nearest-neighbor current-smoothing. The 1D-PIC is actually performed as a very narrow 2D simulation that forbids the growth of transverse modes but allows for statistics similar to full 2D. A careful numerical treatment is required as even
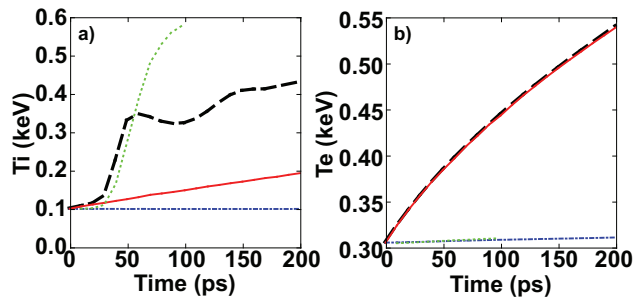
FIG. 4. (Color Online) Evolution of the (a) C^{6+} ion temperature (starting at 0.1 keV) and (b) electron temperature (starting at 0.3 keV) . The dash-dotted blue line corresponds to a 1D collisionless run showing numerical stability; The red lines are a 1D collisional run showing strong resistive heating of the electrons (b) and weak collisional heating of the ions (a); the green dotted line (a) is a 2D collisionless run showing transverse ion heating that follows electron temperature increase; the dashed black lines are a 2D collisional run in which $T_{i\perp}$ is strongly coupled both to T_e (via the instability) and $T_{i||}$ (via i-i collisions).

a very small fraction of the flow energy transferred by scattering on spurious numerical field fluctuations will overwhelm the energy balance of the cold plasma.

To separate the collisional and kinetic effects, we have performed a series of one and two dimensional PIC simulations with and without binary collisions, the initial parameters listed above. N_e is kept constant at 4×10^{18} cm^{-3}. We artificially increase the collisional rates by using a Coulomb logarithm $\ln\Lambda = 32$ instead of ≈ 8 for our parameters to shorten the simulation time to 2×10^6 steps on 1200 processors. Fig. 4 compares the evolution of the electron and ion temperature under various approximations. The 1D-PIC (collisionless) results confirms that numerical heating is negligible and the simulation is stable. In this limit, the 2-stream instability cannot develop because unstable perturbations propagate almost normal to the axis and both T_e and T_i remain constant at small levels. The 1D-Coll-PIC (Coll denotes collisional) shows a fast increase in T_e (Joule heating) and a small increase in T_i (small angle scattering), consistent with the estimate above and Ref. [14]. Fig. 4 (a) shows the evolution of the ion temperature. The evolution of T_e, shown in Fig. 4 (b), is independent of the dimensionality (and of the evolution of T_i) as there is negligible collisional coupling between ions and electrons. The 2D-PIC simulation shows a sudden increase in the transverse ion temperature $T_{i\perp}$ due to the 2-stream instability, followed by saturation at the marginal stability threshold $T_{i\perp} \approx T_e$. $T_{i||}$ remains constant in this supersonic regime as well as T_e.

Finally, the 2D-Coll-PIC simulations reproduces the experimentally observed evolution. While T_e increases due to friction, the 2-stream transfers energy to ions to keep the system close to the marginal threshold $T_{i\perp} \approx T_e$,

and i-i collisions equilibrate $T_{i\perp}$ and $T_{i||}$. In all cases, the conversion of flow energy into electron and ion thermal energy by collisions and plasma instability, while having a dramatic effect on the plasma parameters, remains negligible relative to the total kinetic energy in the flow and no significant slow down nor stagnation is observed.

In order to model the experiment, the density is increased with time in an adiabatic way following the measured density evolution, by increasing the particle weight. This maintains the correct collisional rates, kinetic growth rates and heat capacity of the system. The resulting evolution of T_e and T_i, shown in Fig. 3, are in good agreement with the experiment. One could speculate that the slightly lower T_i simulated at late times could be due to the Weibel instability slowly developing at long wavelength (larger than our simulation box) or the development of intra-jet shocks due to non-uniformaties in the density [22] . On the other hand, the simulation lacks heat conduction and adiabatic cooling at large scale, hence the slight overestimate of T_e at late times.

In conclusion, we have accurately measured the plasma ion and electron temperatures, the flow velocity, and electron density in the interaction region between two collisionless counter-stream plasmas. A rapid increase in both ion and electron temperatures are observed. A series of detailed simulations have been performed and only the simulation including both collisional and collisionless (collective) effects accurately reproduce the measured ion heating.

[1] R. Bosch, *et al.* Physics Of Fluids B-Plasma Physics **4**, 979 (1992).

[2] P. Hough, *et al.* Journal Of Physics D-Applied Physics **42**, 055211 (2009).

[3] R. Berger,*et al.* Physics Of Fluids B-Plasma Physics **3**, 3 (1991).

[4] A. Bell, *et al.* Physical Review A **38**, 1363 (1988).

[5] H.-S. Park, *et al.* High Energy Density Physics **8**, 38 (2012).

[6] H. Takabe, *et al.* *Plasma Physics and Controlled Fusion* (Osaka Univ, Inst Laser Energet, Suita, Osaka 5650871, Japan, 2008) pp. 124057.

[7] T. Morita, *et al.* Physics Of Plasmas **17**, 122702 (2010).

[8] Y. Kuramitsu, *et al.* Physical Review Letters **106**, 175002 (2011).

[9] D. W. Koopman and D. A. Tidman, Physical Review Letters **18**, 533 (1967).

[10] N. C. Woolsey, *et al.* Physics Of Plasmas **8**, 2439 (2001).

[11] T. N. Kato and H. Takabe, Physics Of Plasmas **17**, 032114 (2010).

[12] L. Gargate and A. Spitkovsky, Astrophysical Journal **744**, 67 (2012).

[13] P. W. Rambo, S. C. Wilks, and W. L. Kruer, Physical Review Letters **79**, 83 (1997).

[14] J. S. Ross, *et al.* Physics Of Plasmas **19**, 056501 (2012).

[15] D. H. Froula, J. Sheffield, and S. H. Glenzer, *Plasma Scattering of Electromagnetic Radiation*, Theory and Measurement Techniques (Academic Press, 2010).

[16] S. H. Glenzer, *et al.* Physics of Plasmas **6** (1999).

[17] J. Dardis and J. T. Costello, Journal of Computational Physics **65**, 627 (2010).

[18] D. W. Forlund and C. R. Shonk, Physical Review Letters **25**, 1699 (1970).

[19] J. D. Huba, *NRL Plasma Formulary* (Washington, DC, 2000).

[20] A. J. Kemp, B. I. Cohen, and L. Divol, Physics of Plasmas **17**, 056702 (2010).

[21] T. Takizuka and H. Abe, Journal of Computational Physics **25**, 205 (1977).

[22] D. D. Ryutov,*et al.* Physics Of Plasmas **19**, 074501 (2012).